Mater Renew Sustain Energy (2012) 1:3
DOI 10.1007/s40243-012-0003-9

REVIEW PAPER

Photoreaction of Au/TiO_2 for hydrogen production from renewables: a review on the synergistic effect between anatase and rutile phases of TiO_2

K. Connelly · A. K. Wahab · Hicham Idriss

Received: 9 October 2012 / Accepted: 29 October 2012 / Published online: 28 November 2012
© The Author(s) 2012. This article is published with open access at Springerlink.com

Abstract The review focus is on hydrogen production from renewables using photocatalysis. In particular we focus on the role of synergism on the reaction rate. Among the most studied examples for this phenomenon are catalysts based on TiO_2. TiO_2 exists in two common phases: anatase and rutile, with the latter more thermodynamically stable. For hydrogen production the photocatalyst is often composed of nano-size precious metals deposited on TiO_2 (such as Pt, Pd, or Au). It has been observed by many researchers over a decade that M/TiO_2 rutile is far less active than M/TiO_2 anatase. Yet, the presence of the two phases together results in considerable enhancement of the reaction rate when compared to M/TiO_2 anatase alone. The main reason for this is the increase of the charge carriers' lifetime allowing for electron transfer to hydrogen ions and hole transfer to oxygen ions (and/or the sacrificial agent used). In this work we review the few proposed models, so far, explaining the way by which this charge transfer occurs across both phases.

Keywords TiO_2 anatase · TiO_2 rutile · Hydrogen production · Synergism · Synergistic effect · Ethanol reactions · Water splitting

K. Connelly · H. Idriss (✉)
Department of Chemistry,
University of Aberdeen,
Aberdeen AB24 3UE, UK
e-mail: idrissh@sabic.com; h.idriss@abdn.ac.uk

A. K. Wahab · H. Idriss
SABIC T&I and CRI,
Riyadh and KAUST,
Riyadh, Saudi Arabia

Introduction

TiO_2 has many properties that make it effective for use as a photocatalyst. It is cost effective, abundant, has good surface stability, is non-corrosive, environmentally friendly and has great versatility in its application [1]. Furthermore, due to the position of the conduction band (CB) and valance band (VB) of TiO_2 in relation to a large selection of redox potentials, TiO_2 also shows activity for a large number of surface reactions [2]. Research into the use of TiO_2 as a means for generating hydrogen was initially accelerated by the work of Fujishima and Honda in the 1970s. This work involved photocatalysis to break down H_2O using an electrochemical cell with a TiO_2 electrode connected to a platinum electrode via an external circuit. Fujishima and Honda found that when the TiO_2 electrode was exposed to UV light, a current was established. This was due to the formation of electron-hole pairs, with the current direction indicating oxidation occurred at the TiO_2 electrode and reduction at the platinum electrode [3]. Since this discovery there has been a proliferation of work conducted in the field of photocatalysis, using TiO_2 and other semiconductors, for the intention of hydrogen generation.

Currently the most economically and energetically viable hydrogen production methods are from unsustainable hydrocarbon reforming. However, even methane reforming is currently around four times more expensive than current methods for producing gasoline with the same energy value [4]. The more integral problem with steam methane reforming is that it is clearly unsustainable in the long term. More sustainable methods, such as those utilising renewable feedstock's such as biomass or water, are presently unfeasible because of economics, incomplete technologies and/or low production yields. However, due to the inexhaustible global supply of water, as well as the greater

accessibility of biomass to the majority of the population in comparison to hydrocarbons, the benefits of using a purely renewable feedstock for H_2 production have far reaching implications.

To date there has been a far greater amount of work conducted using powdered TiO_2-based photocatalytic materials than on single crystals. This is because working with single crystals under ultra-high vacuum conditions is currently rather limited because of the technical difficulties associated with conducting these types of experiments. Another limiting factor is the availability of TiO_2 anatase single crystals compared to the rutile ones. As will be discussed in the case of the hydrogen production from organic compounds (as well as water), the rutile phase is largely inactive. This is not necessarily the case for photo-oxidation of organic compounds using molecular oxygen. Because of the very high affinity of O_2 to electrons from the CB of TiO_2, both anatase and rutile have shown high activity, albeit the anatase phase was generally seen to be more active. Photoreaction/oxidation of alcohols, carboxylic acids, acetaldehyde and acetone as well as for smaller molecules such as H_2O, O_2 and CO over the single crystal rutile TiO_2 (110) surface has been studied. Most of these results have been discussed in recent reviews [5–9]. Other recent reviews on photoreaction of powder systems are available and these include those of references [10, 11].

In this review, after a brief presentation of the photocatalytic process with renewables, we will focus on the synergistic effect between TiO_2 anatase and TiO_2 rutile for photoreaction as it is an intriguing phenomenon that may yield considerable activity once well understood.

Au/TiO_2 nanoparticles

TiO_2 alone is not efficient for the photo production of hydrogen from water with or without sacrificial agents (such as methanol, ethanol or glycols) [12]. The effect of the addition of noble metals to TiO_2 has been studied by many groups as it considerably increased the hydrogen production rate. Among the most interesting of them is gold nanoparticle interaction with TiO_2. This review will focus on Au/TiO_2 because the available data allow for a systematic extraction of information. The introduction of Au nanoparticles (NPs) dispersed onto TiO_2 has been found to increase reaction efficiency by facilitating electron transfer and therefore inhibiting electron-hole recombination, as shown in Fig. 1, and by reducing the overpotentials for H_2 generation [13, 14].

The Fermi level (E_f) of Au NPs lies slightly lower than the E_f of TiO_2 and therefore photo-excited electrons can migrate from TiO_2 to surface Au NPs until the two E_fs are aligned with each other. This then allows for photo-

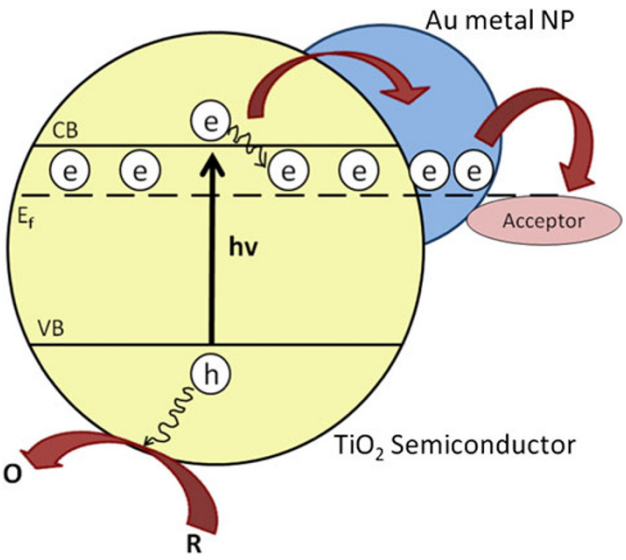

Fig. 1 Enhancement of photo-excitation due to Au nano particles acting as an electron acceptor. Adapted from [14]

generated holes in TiO_2 to migrate to the surface rather than recombining with electrons. The resultant Schottky barrier formed at the Au/TiO_2 interface serves as an efficient electron trap enabling charge separation, and inhibition of recombination, as well as the potential for localised reduction of adsorbates on surface Au NPs [15, 16]. Evidently good interfacial contact between Au NPs and TiO_2 is critical when synthesising Au/TiO_2 photocatalysts. Au/TiO_2 also potentially has the ability to increase the photo-response of TiO_2 into the visible light region because of the Au absorption band lying at 500–600 nm, which is inferred to be the surface plasmon band. It is proposed that excitation of electrons at the surface plasmon band of Au could allow for electron transfer to the low-energy CB of TiO_2, which is photocatalytically inactive with visible light, therefore also providing charge separation [17–21]. Au NP size, dispersion, loading and NP-support interaction all play critical roles in the photocatalytic activity of Au/TiO_2 with all these parameters dependent upon the catalyst preparation methods [17, 22–24]. Among the many methods of preparing Au, particle deposition–precipitation of Au onto TiO_2 provides the good interfacial contact necessary for photocatalytic activity from Au/TiO_2 as initially observed by Bamwenda et al. [22, 24] when comparing various Au/TiO_2 photocatalyst preparation methods.

Bamwenda et al. [22] used UV light to irradiate suspensions of TiO_2 with various Au loadings and monitored H_2 production from a water–ethanol solution. Below are the proposed chemical equations for H_2 evolution. Following electron-hole formation under UV light, electrons are trapped at Au NPs and reduce protons to produce H_2 gas as shown in Eqs. 1–4:

$$e^-(Au_{tr}) + H^+(sol) \rightarrow H\,(ad) \quad (1)$$

$$2H\,(ad) \rightarrow H_2(ad) \quad (2)$$

$$H_2(ad) \rightarrow H_2(sol) \quad (3)$$

$$H_2(sol) \rightarrow H_2(g) \quad (4)$$

where (Au_{tr}) is an electron trapped at an Au site, (sol) is solution, (ad) is adsorbed and (g) is gas phase.

The corresponding surface trapped holes would interact with either water or ethanol, as shown in Eqs. 5–6, as previously suggested by Sakata and Kawai for H_2 production over Pt/TiO_2 from a water–ethanol solution: [27]

$$2h^+_{tr} + C_2H_5OH \rightarrow 2H^+ + CH_3CHO \quad (5)$$

$$2h^+_{tr} + CH_3CHO + H_2O \rightarrow 2H^+ + CH_3CHOOH \quad (6)$$

The acetic acid produced in Eq. 6 can then be decomposed into methane and CO_2 as per the photo-Kolbe reaction shown in Eq. 7 ($CH_3^{\cdot}$ may combine with $H^{\cdot}$, giving CH_4, or with another $CH_3^{\cdot}$ to give C_2H_6), with methane also possibly forming via Eq. 8:

$$h^+_{tr} + CH_3COO\,(ad)\cdot \rightarrow CO_2 + CH_3^{\cdot} \quad (7)$$

$$CO_2 + 4H_2 \rightarrow CH_4 + H_2O \quad (8)$$

By depositing precious metal onto the TiO_2 surface, it was suggested that the higher E_f of the semiconductor compared to that of the metal allows for smooth electron transfer from TiO_2 to the metal and resulted in the formation of a space charge layer at the metal side of the interface [26]. This space charge layer causes charge carriers to be transported in opposite directions and therefore reduces the probability of recombination [27].

Previous work by our group has so far focused on hydrogen production from ethanol over Au-loaded anatase and rutile powdered catalysts. Nadeem et al. [28] investigated the effect of varying the anatase particle size from nanoparticle to microparticle, with Au NPs of the same size, on H_2 rates from ethanol in order to determine the effect of support particle size on the reaction. Upon normalisation of the H_2 rate with respect to the surface areas of the TiO_2 nano- and micro-particles, it was found that both particle sizes yielded similar specific reaction rates, indicating that support particle size is not an important parameter for Au/TiO_2 photocatalysis. Infrared spectroscopy (IR) of the ethanol exposed Au/TiO_2 surface showed deprotonation of ethanol upon ethanol adsorption on the Au/TiO_2 surface, similar to most metal/metal oxides systems [29, 30]. Combining the IR data with the desorption profile gained from temperature programmed desorption (TPD), which showed the main reaction to be that of dehydrogenation of ethanol to form acetaldehyde, Nadeem et al. [28] put forward the following reaction pathway for the photoreaction of ethanol over the Au/TiO_2 surface as shown in Eqs. 9–11. During the process each ethoxide injects two electrons into the TiO_2 CB to produce an α-hydroxyethyl radical (Eq. 10a) and acetaldehyde (Eq. 10b).

$$CH_3CH_2OH\,(ad) + Ti^{4+}{-}O^{2-}(s) \rightarrow CH_3CH_2O^-{-}Ti^{4+}(ad) + O{-}H\,(ad) \quad (9)$$

$$CH_3CH_2O^-{-}Ti^{4+}(ad) + 1h^+ + O^{2-}(s) \rightarrow CH_3CH^{\cdot}O{-}Ti^{4+}(ad) + O{-}H\,(ad) \quad (10a)$$

$$CH_3CH^{\cdot}O{-}Ti^{4+}(ad) + 1\,h^+ \rightarrow CH_3CHO\,(g) + Ti^{4+}(s) \quad (10b)$$

$$2O{-}H\,(ad) + 2e^- \rightarrow 2O^{2-}(s) + H_2\,(ad) \quad (11)$$

The production of H_2 in this scheme requires some of the photoexcited electrons to migrate from the TiO_2 CB to become trapped at Au NPs, which, if in the vicinity of H^+ ions produced from the deprotonation of ethanol upon adsorption, can reduce the protons to form H_2 gas.

This reaction mechanism was further refined by Murdoch et al. [31] when investigating various loadings of Au on both rutile and anatase NPs. The anatase supports had Au particle sizes between ~3 and 20 nm, whilst the rutile supports had Au particle sizes between ~20 and 35 nm. Negligible photoactivity for the production of H_2 from ethanol was observed for the un-doped rutile and anatase photocatalysts alone. The results from loading Au onto the anatase and rutile supports and running the photoreaction are shown in Fig. 2 with the H_2 rate pertaining to anatase on the left axis and the H_2 rate for rutile on the right. From Fig. 2 it can be seen that Au loaded onto anatase NPs led to an increase in the H_2 rate to a maximum of 1.1×10^{-6} mol $m^{-2}_{cat.}$ min^{-1} with increased loading up to 4 wt% Au, after which the H_2 rate decreases. For Au loaded onto rutile hydrogen production is far lower, about two orders of magnitude lower than that on anatase (1.7×10^{-8} mol $m^{-2}_{cat.}$ min^{-1}). The two orders of magnitude

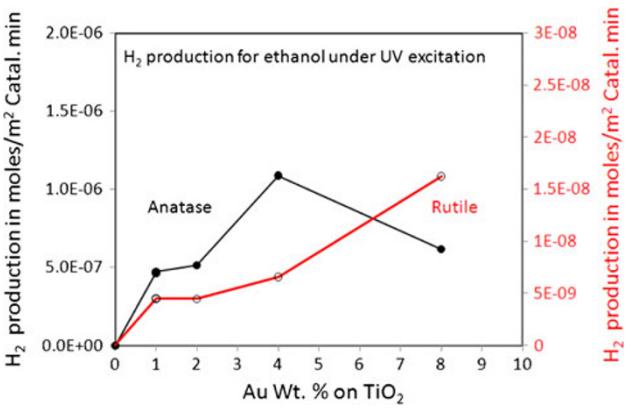

Fig. 2 Photocatalytic H_2 production from ethanol over Au/TiO_2 anatase (A) and rutile (R) as a function of wt% Au loading [29]

difference between the H_2 rates, produced over the rutile and anatase catalysts, were explained to be due to the greater charge recombination rate of rutile as compared to anatase. For the 1, 2 and 4 wt% Au/anatase catalysts, Murdoch et al. normalised the H_2 rates to the number of exposed Au atoms on the surface, calculated from XPS data of Au4f. They found the normalised rate to be independent of Au particle size. This is in contrast to results observed for dark reactions where increasing Au particle size above around 4 nm results in a decrease in the catalytic activity [32–35].

Rutile and anatase polymorphs of TiO_2

There are several main differences between the anatase and rutile phases of TiO_2. First, the band gap (BG) of rutile is slightly smaller at 3.0 eV as compared to 3.2 eV for anatase [23]. Anatase can therefore only be excited by UV light whilst rutile has a photo-response to UV light, as well as extending slightly into the visible light region [36]. It is generally accepted that the CB of anatase lies higher than that of rutile [37]; however there is still some debate about the relative positions between the anatase and rutile CBs [38], as well as the exact CB potentials for both of these TiO_2 polymorphs [39–41]. Furthermore anatase has an indirect BG whilst rutile has a direct BG, which may affect electron-hole recombination rates. Many authors have studied the kinetics and mechanisms of charge separation and electron-hole recombination in rutile and anatase. Colbeau-Justin and Kunst [42] used a time-resolved microwave conductivity (TRMC) method to probe charge carrier lifetimes in TiO_2 with the TRMC signal attributable to electron activity because electron mobility is greater than that of the associated holes. From the TRMC signal it was evident that rutile showed faster decay of mobile electrons than observed for anatase. This demonstrates that rutile has a shorter photoexcited electron lifespan and therefore higher recombination rate in relation to anatase, whilst anatase charge carriers are subjected to competition between recombination and hole trapping processes allowing for a longer lifespan of charge carriers. Upon exposure of anatase to ethanol, the TRMC signal showed a much slower decay inferring that ethanol is scavenging holes at the surface and trapping them there. For rutile exposed to ethanol no difference was observed to the signal recorded for unexposed rutile, further indicating that fast recombination is occurring. Using the same method Xu et al. [43] confirmed these findings using single crystals of rutile (110) and anatase (101). As shown in Fig. 3, there is a difference in the observed signal of around one magnitude between both crystals. The signal for rutile rapidly decays, even during the excitation period, and therefore indicates that fast electron-hole recombination has occurred. Conversely the slower signal decay observed for anatase, as well as the much larger signal amplitude, shows that anatase charge carriers have a lifetime of over 10 ns. This difference in charge carrier lifetimes between these two TiO_2 polymorphs has been attributed by the authors to the differing band structures presumed to arise in anatase and rutile, as shown in the inset in Fig. 3. It is envisioned that in anatase, with an indirect BG as opposed to the direct BG in rutile, following the vertical photoexcitation of electrons into the unoccupied states of the anatase CB electrons then relaxing to the bottom of the CB will be unable to undergo direct recombination with holes because of the indirect BG. This consequently would lead to longer charge carrier lifetimes and an increase in the diffusion length of electron-hole pairs excited within the bulk. Equally important, the CO photo-oxidation was conducted on both surfaces using reflection absorption infrared spectroscopy (RAIRS). TiO_2(101) anatase was found to be about eight times more photo-catalytically active than TiO_2(110) rutile.

Using TiO_2 films Shen et al. [44] directly measured the photoexcited hole activity of both rutile and anatase phases using a lens-free heterodyne detection transient-grating (LF-HD-TG) method. The LF-HD-TG signal is attributed to the change in the amount of photoexcited holes as the effective mass for holes is far smaller than that for electrons. Upon laser excitation the anatase signal quickly decreased (<2 ps) and was followed by a slow decay thereafter, whilst the rutile sample showed only a slow decay. The rapid decrease of the anatase signal was of first-order kinetics and proposed to be due to surface hole trapping whilst the slow decay observed for both samples indicative of recombination and/or trapping processes occurring within the bulk of the particles. Experiments

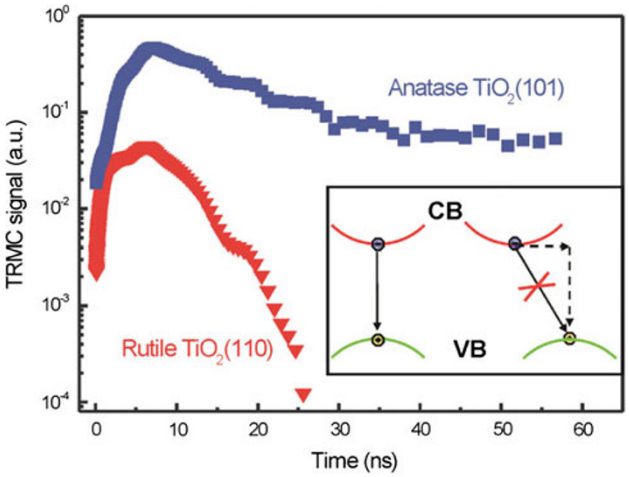

Fig. 3 Transient photoconductance measurements at 30 GHz using 355-nm laser pulses (10-ns FWHM) in rutile (110) and anatase (101) single crystals. The *inset* shows a schematic of the proposed model of the rutile band gap (*left*) and the anatase band gap (*right*) [43]

were also run on anatase and rutile of various NP size, which showed the same LF-HD-TG response regardless of particle size. Based on these findings Shen et al. proposed that the differences in the charge dynamics observed between rutile and anatase could be dependent on the difference in the dielectric constants of the two phases. Surface potential barrier height is inversely proportional to the dielectric constant and so the smaller dielectric constant of anatase gives rise to a larger surface potential barrier, with the potential slope being steeper for anatase than for rutile, as shown in Fig. 4. This results in the faster transport of holes to the surface of anatase than in rutile, with subsequent hole trapping at surface sites, which correlates with the initial fast decay of the signal upon excitation of anatase.

Work was conducted on the photocatalytic reaction of acetic acid over the rutile (011) surface reconstructions {011} and {114} [45, 46]. The {011} surface was found to be far more active for this reaction than the {114} surface, and upon calculating the depletion layer from the quantum yield of the reaction from both surfaces it was found that the more reactive {011} reconstruction had a larger depletion layer and therefore higher potential barrier height than the {114} surface. The increase of reactivity observed as being proportional to the depletion layer was attributed by these authors as being due to the width of the depletion layer affecting the electron-hole recombination rate, which correlates with the work of Shen et al. [44].

TiO_2 P25: a case study for the synergistic effect in photocatalysis

TiO_2 P25 is the industry standard, mixed phase rutile/anatase TiO_2 catalyst that has repeatedly shown enhanced catalytic activity in comparison to using the rutile and anatase phases alone. P25 has an anatase/rutile ratio of ~70/30 with a surface area of typically 50 ± 15 m^2 g^{-1} [36]. The method used for synthesising P25 must ensure good contact between anatase and rutile in order to observe the synergistic effect between the two phases. The preparation method of the catalyst will also have a direct effect

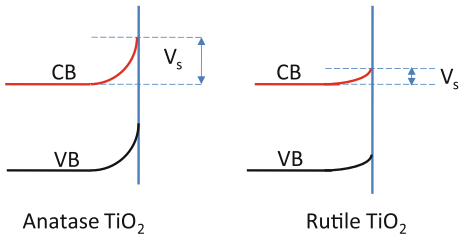

Fig. 4 Schematic of surface band bending in anatase and rutile, V_s is the surface potential barrier height; adapted from [44]

on the morphology of the interfacial boundaries, in turn affecting the electronic energy levels of electron-hole pairs [45]. Furthermore the calcination temperature of the catalysts must be closely controlled in order to gain the required TiO_2 phase composition, with phase transformation of anatase to rutile beginning at around 550 °C [46].

Several authors have monitored H_2 production from various reactants over mixed phase TiO_2 photocatalysts. Zhang et al. [46] deposited Pt onto almost pure rutile, pure anatase and mixed phase TiO_2. Surface phase composition of the TiO_2 particles was controlled by increasing the calcination temperature and confirmed using XRD, visible and UV Raman spectroscopy. At 550 °C the anatase phase in the bulk began to transform to rutile with the surface retaining the anatase phase until temperatures above 680 °C. Above 700 °C nearly all bulk anatase is transformed into the rutile phase and around 44 % of surface anatase remains. Complete phase transformation to rutile is achieved upon calcination to 800 °C. From monitoring H_2 production from the reaction of methanol and water over these TiO_2 photocatalysts, the H_2 rate with respect to the surface specific area of the catalyst was calculated. The highest activity observed was for the photocatalyst calcined at 700–750 °C (rutile bulk and mixed phase surface), which yielded a H_2 rate around four times greater than that observed for rutile alone. From UV Raman spectra of the 700–750 °C calcined catalysts, the authors confirm that both rutile and anatase coexist at the surface and therefore have surface phase junctions. It has been postulated by many authors [23, 25, 39, 46–48] that it is the presence of surface phase junctions in mixed phase TiO_2 that facilitates the electron transfer between the two phases upon photoexcitation and therefore improves charge separation, reduces recombination and subsequently increases photocatalytic activity.

Kho et al. [39] measured the onset potentials versus Ag/AgCl of mixed phase TiO_2 NPs and found that above 60 % anatase content there is a steady increase in the onset potential observed. The onset potential can be taken as an evaluation of the quasi-E_f of the photocurrent from the anode and therefore Kho et al. suggested that E_f band bending had occurred, which would indeed require intimate contact between the two TiO_2 phases. The authors also monitored H_2 production over a TiO_2 suspension with an aqueous solution of methanol and H_2PtCl_6. Within the TiO_2 suspension the anatase/rutile content was varied, and an optimum anatase content of 39 % was found to yield the best H_2 rate in comparison to pure rutile or anatase as well as other phase composites. Based on the 39 % anatase composition another catalyst was prepared via manual grinding of anatase and rutile samples and tested for H_2 production. This time no synergistic effect was observed between anatase and rutile, showing that the grinding

method did not produce sufficient inter-particle mixing, and therefore no good interfacial contact was made between the two phases, which is crucial for the enhanced photocatalytic activity that was previously observed. Kho et al. described the mechanisms for the synergistic effect between anatase and rutile in the presence of methanol as shown in Fig. 5. Electron-hole pairs are generated after photoexcitation in both anatase and rutile with methanol acting as a hole scavenger and oxidised at the VB of both anatase and rutile. Due to the lower potential of the rutile CB, as compared to the anatase CB, Kho et al. proposed that the majority of photoexcited electrons at the anatase CB migrate across the phase junction to the rutile CB. Therefore, the majority of H^+ ion reduction occurs at the rutile CB, with a smaller amount occurring at the anatase CB. Due to this transfer of electrons from the anatase CB to the rutile CB, the likelihood of electron-hole recombination at either the anatase or rutile VBs would be decreased with more H^+ reduction occurring at the rutile CB than would be observed in single-phase rutile. However, due to the rutile CB minimum being closer to the H^+ reduction potential than that of the anatase CB, there is possibly no benefit to be gained from transferring photoexcited electrons from the anatase to rutile CB for H^+ reduction and in fact another mechanism for the observed synergistic effect in P25 could be occurring.

From work on the photooxidation of phenol by various pure and Pt doped TiO_2 P25 and Hombikat UV100 (HK) photocatalysts, Sun et al. [23] found that TiO_2 P25 alone showed the greatest phenol degradation. According to Sun et al. band bending caused by interfacial contact between the two phases resulted in the anatase CB energy increasing within the space charge layer and therefore prohibiting electrons from migrating from anatase to rutile, as shown in Fig. 6. However VB bending of both phases allows for hole migration from the anatase to the rutile VB, explaining P25's enhanced photoactivity in liquid reaction. This would result in holes mostly populating the rutile VB where the majority of oxidation would occur and electrons concentrated at the anatase CB where mostly reduction reactions would occur. It is thought that rutile's role in the process is purely for charge separation and providing oxidation sites. Photoexcited electrons in rutile are not thought to be directly involved in the reaction and instead undergo recombination with holes.

Other TiO_2 systems studied for the synergistic effect in photocatalysis

Using theoretical studies Deak et al. [38] produced the generic band alignment scheme shown in Fig. 7. It was found that the rutile CB lay higher than the anatase CB by around 0.3–0.4 eV, whilst the anatase VB is around 0.5–0.6 eV lower than for rutile. This is in disagreement with other models discussed already whereby the rutile CB is lower in energy than the anatase CB [23, 39]. Despite this, the authors concluded that this band alignment will result in an accumulation of migrating electrons at the anatase CB and migrating holes at the rutile VB; the latter is in agreement with several other studies [25, 49–52].

Further models that have gained greatest acceptance are commonly referred to as the 'rutile antenna' and the 'rutile sink' models [25]. Bickley et al. [49] proposed the 'rutile sink' model as shown in Fig. 8. In this model Bickley et al. assumed there to be an overlayer of rutile on the anatase and that <1 % of UV radiation was absorbed by the rutile overlayer. On this assumption the majority of incident light is absorbed by, and photoexcited electrons in, the underlying anatase. In agreement with Sun et al. [23], it is thought that when the E_fs of both phases are in contact with each other a space charge layer is created promoting the migration of holes from anatase to rutile and then to the surface, as shown in Fig. 8. Due to the position of the CB

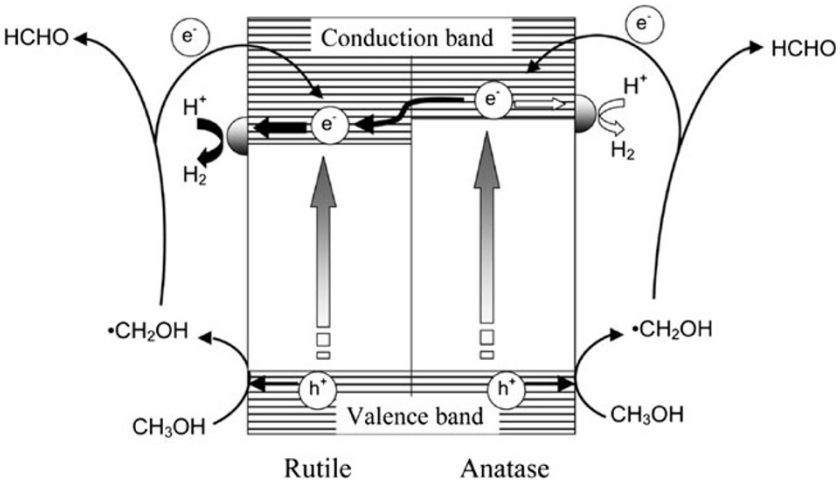

Fig. 5 Schematic of the electron pathway during the photocatalytic production of H_2 over anatase and rutile particles [39]

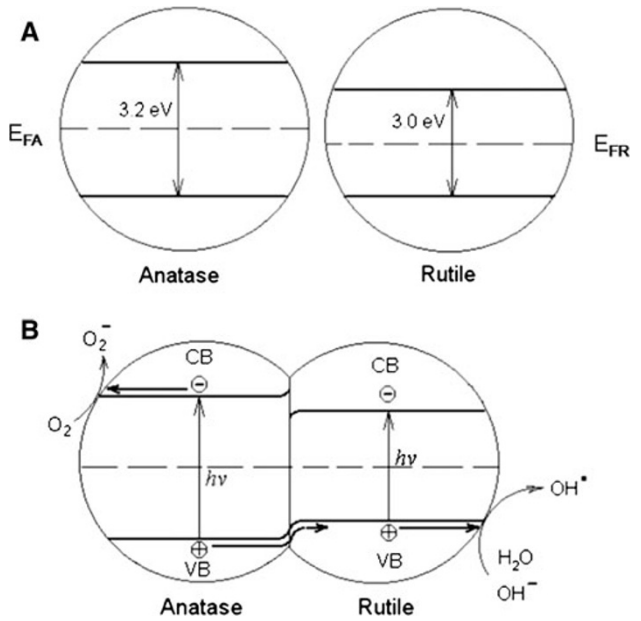

Fig. 6 Mechanism proposed for electron-hole separation in P25 following photo-excitation; adapted from [24]. **a** Before anatase and rutile phases contact each other. **b** After the line up of Fermi levels of anatase and rutile phases

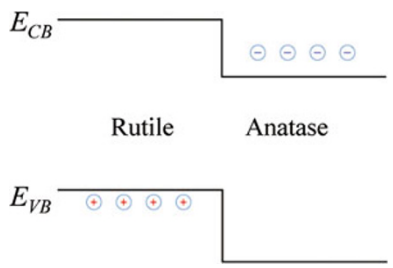

Fig. 7 Schematic of rutile/anatase band alignment [38]

edges and E_f of the two phases, the space charge layer is thought to adversely affect the migration of electrons toward the surface. However, electron migration from the lower energy rutile CB to the higher energy anatase CB, as shown in Fig. 8 by Bickley et al. [49], is energetically unfavourable.

Scott et al. [52] obtained H_2 production rates of the ethanol reaction over pure phase Au/rutile and Au/anatase, as well as for Au/P25. It was found that when the H_2 rates were normalised, in order to take into consideration the number of exposed Au atoms on the surface, that 1.5 wt% Au/P25 had a H_2 rate (7×10^{-5} mol^{-1} m^2 min^{-1}) that was around two times greater than that seen for 2.0 wt% Au/Anatase (4×10^{-5} mol^{-1} m^2 min^{-1}), which was found to have a rate of two orders of magnitude greater than that observed for 2.0 wt% Au/Rutile (6×10^{-7} mol^{-1} m^2 min^{-1}). Scott et al. proposed that the synergistic mechanism operating in P25 that led to the enhancement of the H_2 rate involves electron transport from the rutile phase to the anatase phase. They

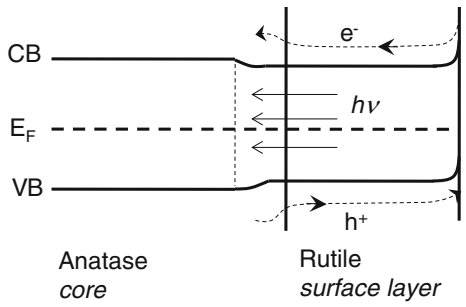

Fig. 8 Mechanism for the synergistic effect of a thin overlayer of rutile on anatase; adapted from [49]

propose that the smaller BG of rutile results in the generation of a higher number of charge carriers in rutile than observed in anatase and that these electrons are then transferred to the anatase CB where they benefit from a slower rate of electron-hole recombination; Fig. 9. The enhanced H_2 rate observed for P25 can then be attributed to the reaction occurring mainly at the anatase CB where there is a greater difference in the potentials of the anatase CB and the redox potential for H^+ reduction than is the case for the rutile CB and H^+ reduction potential.

Hurum et al. [50] re-evaluated this 'rutile sink' model using electron paramagnetic resonance (EPR) spectroscopy following visible light photoexcitation in order to take into account any charge transfer trapping on charge carrier pathways. EPR can be used to focus on the electron and hole trap population and recombination behaviour in mixed phase TiO_2 and is very useful in this respect as it is able to directly and indirectly detect photo-induced radicals via spin-trapping methods allowing for the identification of electron and hole surface and lattice trapping sites [37]. Upon irradiation of the aqueous P25 sample with visible light, the signal intensity for the population of anatase bulk and surface trapping sites increased, whilst the rutile trapping site signal simultaneously decreased. This evidence directly indicates that electron transfer is occurring from rutile to anatase under visible light. As Hurum et al. used visible light to excite their samples, rather than UV, only rutile has the potential to utilise the highest frequency light available from the visible light source for photo-excitation. Therefore, photoexcitation would only occur in rutile with these electrons transferred to anatase, specifically to trapping sites that lie just below the anatase CB. As shown in Fig. 10, further electron transport fills up surface trapping sites in anatase, resulting in the availability of photogenerated holes in rutile to be available for oxidative reactions.

Nair et al. [27] also investigated the synergistic effect between anatase and rutile using the photodegradation reaction of phenol under both UV and visible light. As expected under UV light the photocatalysts with the

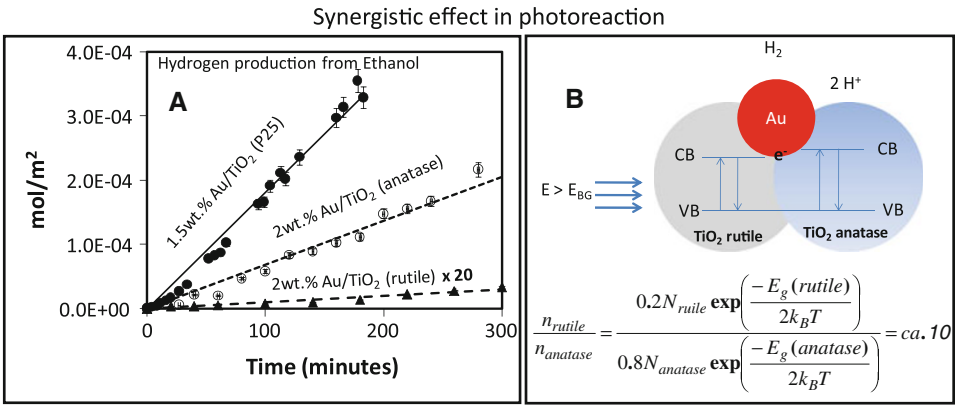

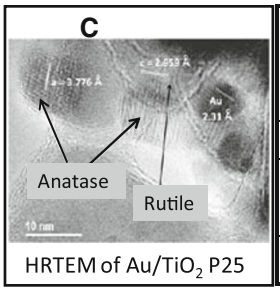

Catalyst	BET m^2/g	Corrected XPS Au4f/Ti2p	Rate mol/(m^2.min)	Normalized rate
Au/TiO_2 (P25)	48	0.024	18×10^{-7}	7×10^{-5}
Au/TiO_2 (anatase)	105	0.017	7×10^{-7}	4×10^{-5}
Au/TiO_2 (rutile)	170	0.008	5×10^{-9}	6×10^{-7}

Fig. 9 **a** Production of hydrogen (per unit area) from ethanol over 1.5 Au wt%/TiO_2 P25, 2 wt% Au/TiO_2 anatase and 2 wt% Au/TiO_2 rutile. **b** Model explaining the role of rutile and anatase as synergistic effect. In the model the larger number of charge carriers in rutile associated with the slower rate of charge carriers disappearance in anatase is behind the high activity of P25. **c** HRTEM of the 2 wt% Au/TiO_2 P25; the interface between Au, anatase and rutile is clearly seen. The table present results from **a** normalised to the surface Au signal from their XPS Au4f. Still after normalisation the rate of Au/TiO_2 P25 is larger than that of Au/TiO_2 anatase. The rate of hydrogen production is negligible

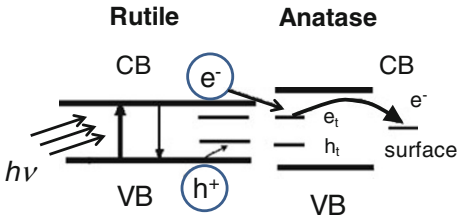

Fig. 10 Rutile antenna model explaining the synergistic effect between rutile and anatase; adapted from [50]

highest anatase content (88 and 92 %) showed the highest activity, whilst under visible light photocatalysts with the highest rutile content (72 and 76 %) showed the highest activity. Nair et al. explained these results by proposing a slightly modified version of the 'rutile sink' and 'rutile antenna' models based on the band structure of the two phases at the phase junction. Figure 11a shows the proposed interfacial band model between rutile with a BG of 3.0 eV and anatase with a BG of 3.2 eV at equilibrium and the potential charge barrier formed at the phase junction. Figure 11b shows the model after UV excitation where excitation of electrons to the CB occurs mainly in anatase. The charge barrier created between the two phases encourages migration of electrons in the interfacial region from the anatase CB to the rutile CB and holes migrate to the anatase VB. Figure 11c shows the model under visible light excitation with a photoresponse only from rutile. This time the charge barrier influences electron transfer in the interfacial region from the rutile CB to the anatase CB with holes remaining at the rutile VB.

Carneiro et al. [51] agree with the work cited in refs. [23, 38, 49] in that hole migration occurs from anatase to rutile in mixed phase TiO_2; however they found that the efficiency of photocatalytic reactions carried out in aqueous liquid phase in the presence of rutile was actually reduced because of this hole migration rather than increased. Carneiro et al. monitored the photocatalytic activity of both methylene blue degradation and cyclohexane oxidation over a series of sol–gel TiO_2 photocatalysts calcined at various temperatures in order to gain various phase compositions. By increasing the calcination temperature the % of rutile increased, along with the particle size of both anatase and rutile, whilst the presence of surface water and hydroxyl groups was observed to decrease because of the decreased surface area. It is proposed that the lower density of OH groups on the rutile surface than observed for the anatase particles means that holes that have migrated to rutile are not being utilised in surface processes, whereas when no rutile is present photogenerated holes will remain at anatase where they can participate in surface reactions. Carneiro et al. [51] suggested that the observed discrepancy between the photoreactivity of their catalysts, as compared to P25, was due to the improved crystalline quality of the TiO_2 particles in P25 and it is therefore anatase particle size and morphology in P25 rather than through charge separation between the two phases that results in the enhanced reactivity observed.

In direct opposition to the majority of previously proposed charge transfer models [38, 49, 50], Scotti et al. [54] used EPR to determine that for hydrothermally synthesised

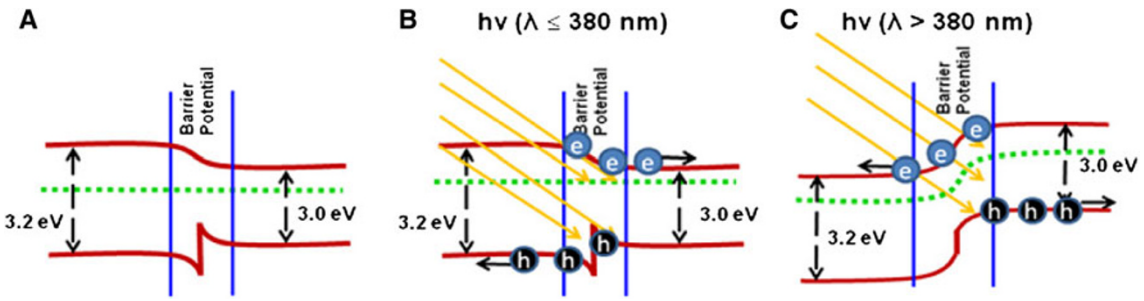

Fig. 11 Proposed interfacial band model, **a** under equilibrium, **b** under UV light and **c** under visible light [28]

mixed phase TiO_2 catalysts UV excited electron transfer was occurring from the anatase to the rutile phase, as previously concluded by Kho et al. [39]. Figure 12 shows the EPR signal for (a) pure rutile, (b) 61 % rutile, (c) 48 % rutile, (d) 20 % rutile and (e) pure anatase at 10 K following UV irradiation for 20 min. From these results it can be seen that the signal obtained for the mixed phase catalysts is similar to that obtained for pure rutile regardless of the anatase % of the catalyst. This indicates that electrons in mixed phase TiO_2 are preferentially trapped at O^- and Ti^{3+} sites on the rutile phase. Scotti et al. therefore conclude that under UV excitation electrons are transferred from the higher energy anatase CB to the lower energy rutile CB, with hole migration simultaneously occurring from the lower energy anatase VB to the higher energy rutile VB.

Komaguchi et al. [47] also show evidence for electron transfer from anatase to rutile due to the presence of trapping sites. Pure phase anatase and rutile as well as P25 catalysts were partially reduced and then subjected to light of wavelength less than the rutile BG. Upon illumination the Ti^{3+} ESR signal for both pure anatase and rutile disappeared and was then restored to full signal intensity upon switching off the light. The photoresponse signal for P25 also disappeared upon illumination; however on turning off the light source the signal exceeded its initial response, reaching 130 % of the initial intensity for the reduced P25 catalyst and 250 % of initial intensity for the air treated P25 catalyst. Furthermore, following restoration of the signal after illumination, the rutile component is observed to be more dominant than previously observed, showing that there is increased electron trapping in rutile. As the light source used in this work is unable to photoexcite electron-hole pairs in TiO_2, Komaguchi et al. proposed that it is trapped electrons that are being excited from trap sites around 0.3–0.8 eV below the CB. Following excitation of trapped electrons into the TiO_2 CB, the ESR signal is unobservable until relaxation of electrons back into Ti^{3+} sites occurs. By taking into account the increase in rutile signal following illumination, the following scheme is suggested, as shown in Eq. 12. First, electrons at anatase trap sites are photoexcited into the anatase CB where the

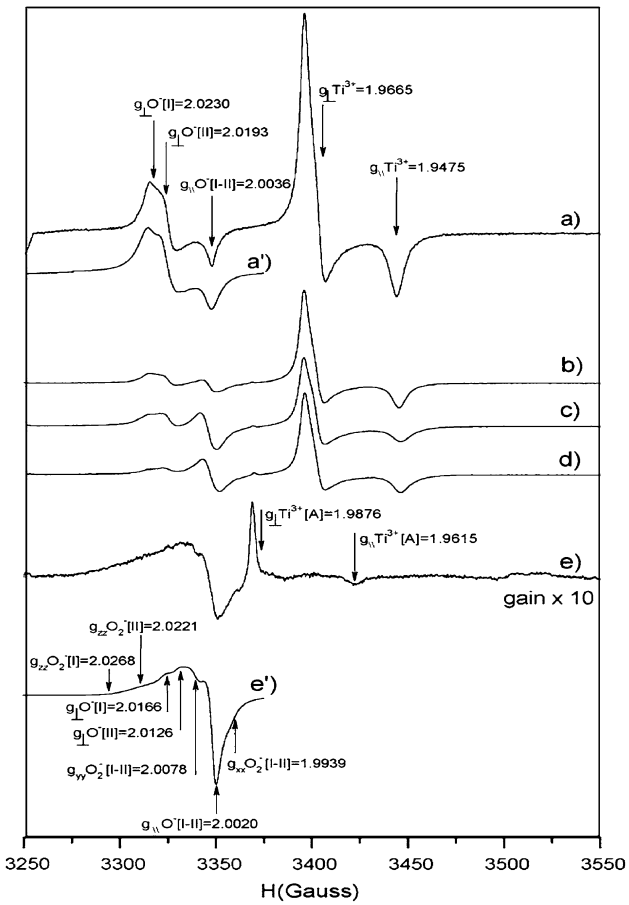

Fig. 12 EPR spectra of hydrothermally synthesised TiO_2 recorded at 10 K following 20 min of UV irradiation showing trapping centres at O^- sites and Ti^{3+} sites. *a* 100 % rutile, *b* 61 % rutile, *c* 48 % rutile, *d* 20 % rutile and *e* 0 % rutile (100 % anatase) [54]

corresponding ESR signal remains silent until the electrons relax and return to trap sites. In this case the majority of excited electrons are transferred to the rutile CB before becoming re-trapped at rutile trapping sites.

$$Ti^{3+}A\,(s) \rightarrow h\nu \rightarrow (e^-_{CB})\,TiO_2A \rightarrow [(e^-_{CB})\,TiO_2R] \rightarrow Ti^{3+}R\,(s) \quad (12)$$

where Ti^{3+}As are anatase electron trapping sites, $[(e^-_{CB})\,TiO_2A]$s are anatase CB electrons, $[(e^-_{CB})\,TiO_2R]$s are

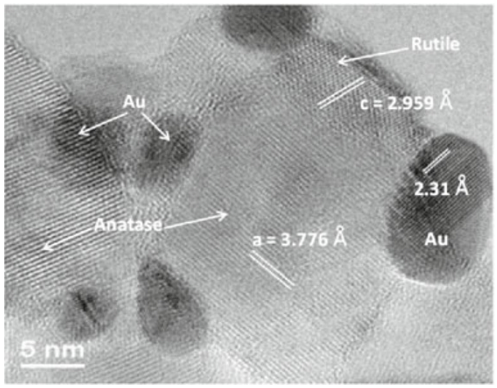

Catalyst	Rate (mole/(m^2_{Catal}.min)	Quantum yield, %	Surface area $m^2/g_{Catal.}$
8wt. % Au/TiO_2 rutile	8×10^{-10}	0.6	168
8wt. % Au/TiO_2 anatase	5×10^{-8}	9	104
8wt. % Au/TiO_2 P25	2×10^{-7}	18.4	48

Fig. 13 HRTEM of 8 wt% Au/TiO_2 P25. Au particles (*dark* particles). The close proximity of anatase, rutile and Au particles ensures electron transfer to reduce hydrogen ions to hydrogen molecules. Despite the high loading of Au the mean particle size is still about 5 nm, evidence of high dispersion. The table presents the rate of reaction, the quantum yield for 8 wt% Au/TiO_2 catalysts and the corresponding surface areas. Flux of UV (360 nm) photons is 1.8×10^{15} photons/s cm^2

rutile CB electrons, Ti^{3+}Rs are rutile electron trapping sites and (s)s are surface ions.

Hurum et al. [53] monitored recombination behaviour of electron-hole pairs at the surface and in the lattice of P25 using EPR. By adding 2,4,6-trichlorophenol (TCP) and then methanol to P25 to act as hole scavengers, the resultant EPR signal should show electrons populating surface trapping sites. Upon illumination with fluorescent light, at room temperature, the EPR signal for anatase surface electron trapping sites is observed to be very broad, indicating that a wide variety of both surface and lattice sites, with varying geometries and therefore energies, have been populated. Also observed is a signal attributed to distorted four-coordinated interfacial sites, as previously observed between silica and anatase coatings. Following illumination of the sample, this time at 10 K, more electron-hole pairs were created because of the lower temperature impeding charge carrier mobility. Subsequently any recombination of trapped species will occur where the electron-hole pair was formed. The resultant EPR signal showed there to be a decrease in both the number of populated surface electron trapping sites and interfacial electron trapping sites, which coincided with an increase in the signal for the anatase and rutile lattice electron trapping sites. These two observations indicate that recombination of electron-hole pairs is dominantly a surface process with photoexcited holes within TiO_2 particles generated on the particle surface and photoexcited electrons quickly trapped at lattice sites. This work directly shows that the surface-to-bulk ratio of particles in photocatalysis influences photoexcitation in particulate systems.

In a very recent work from our group [55], a series of Au/TiO_2 catalysts was studied for TiO_2 anatase, rutile and P25. Au wt% was changed from 1 to 8 %; TEM of Au particles showed a very similar particle size distribution, typically with a mean size between 4 and 5 nm. The quantum yield of the hydrogen production was measured using ethanol (0.5 vol%) as a sacrificial agent under UV excitation of 360 nm with a light flux of about 1 mW/cm^2. Part of the results is presented in Fig. 13. In all cases the rutile quantum yield was found less than 1 % and is therefore of little activity. The quantum yield of the anatase series increased with increasing Au loading. It was found equal to 9 % for 8 wt% anatase. At all Au concentrations the quantum yield of the P25 was found higher than that of the anatase. For example, the quantum yield of 8 wt% Au/TiO_2 P25 was found equal to 18.4 %. This once again is a direct observation of the synergistic effect of the two phases for the reaction.

There are also limited studies on the synergistic effect of TiO_2 phases different from those between anatase and rutile such as between anatase and brookite [56, 57] and rutile-brookite [58] that are treated in this work because of the so far very limited work. Despite the recent increase in studies on the role of each phase, as presented here and elsewhere [58–62], on the possible transfer routes for charge carriers across the mixed phase titania photocatalysts there is still no generally accepted consensus on the exact mechanisms for the synergistic effect between anatase and rutile. The clearest results still indicate that the presence of three phases—nano-particles of the precious metal (such as gold), the rutile and the anatase phase—in intimate contact is needed. Along this interface the transfer of holes from the anatase to the rutile phase appears to be the most plausible [but the transfer of electrons from the rutile to the anatase surface-trapped sites (Figs. 8, 9, 10) or due to a different band bending, interfacial band model (Fig. 11) is still unclear].

Open Access This article is distributed under the terms of the Creative Commons Attribution License which permits any use, distribution, and reproduction in any medium, provided the original author(s) and the source are credited.

References

1. Ni, M., Leung, K.H., Leung, D., Sumathy, K.: A review and recent developments in photocatalytic water-splitting using TiO_2 for hydrogen production. Renew. Sustain. Energy Rev. **11**, 401–425 (2007)
2. Linsebigler, A.L., Lu, G., Yates, J.T. Jr.: Photocatalysis on TiO_2 surfaces: principles, mechanisms, and selected results. Chem. Rev. **95**, 735–758 (1995)
3. Fujishima, A., Honda, K.: Electrochemical photolysis of water at a semiconductor electrode. Nature **238**, 37–38 (1972)
4. Crabtree, G.W., Dresselhaus, M.S., Buchanan, M.V.: The hydrogen economy. Phys. Today **57**, 39–44 (2004)
5. Idriss, H.: Photoreactions of organic compounds with TiO_2 single crystal surfaces. In: Anpo, M., Kamat, P. (eds) Environmentally Benign (Chapter 21), ISBN: 978-0-387-48441-9 (2010)
6. Waterhouse, G.W.N., Idriss, H.: Photoreaction of ethanol and acetic acid over model TiO_2 single crystal surfaces. In: Vayssieres, L (ed) On Solar Hydrogen & Nanotechnology (Chapter 3). Wiley, New York (2009)
7. Henderson, M.A.: A surface science perspective on TiO_2 photocatalysis. Surf. Sci. Rep. **66**, 185–297 (2011)
8. Yates J.T. Jr.: Photochemistry on TiO_2: mechanisms behind the surface chemistry. Surf. Sci. **603**, 1605–1612 (2009)
9. Walter, M.G., Warren, E.L., McKone, J.R., Boettcher, S.W., Mi, Q., Santori, E.A., Lewis, N.S.: Solar water splitting cells. Chem. Rev. **110**, 6446–6473 (2010)
10. Bowker, M.: Sustainable hydrogen production by the application of ambient temperature photocatalysis. Green Chem. **13**, 2235–2246 (2011)
11. Connelly, K.A., Idriss, H.: The photoreaction of TiO_2 and Au/TiO_2 single crystal and powder surfaces with organic adsorbates. Emphasis on hydrogen production from renewables. Green Chem. **14**, 260–280 (2012)
12. Yang, Y.Z., Chang, C.H., Idriss, H.: Photo-catalytic production of hydrogen from ethanol over M/TiO_2 catalysts (M = Pd, Pt or Rh). App. Cat. B Environ. **67**, 217–222 (2006)
13. Mogyorosi, K., Kmetyko, A., Czirbus, N., Vereb, G., Sipos, P., Dombi, A.: Comparison of the substrate dependent performance of Pt-, Au- and Ag-doped TiO_2 photocatalysts in H_2 production and in decomposition of various organics. React. Kin. Cat. Lett. **98**, 215–225 (2009)
14. Subramanian, V., Wolf, E.E., Kamat, P.V.: Catalysis with TiO_2/gold nanocomposites. Effect of metal particle size on the Fermi level equilibration. J. Am. Chem. Soc. **126**, 4943–4950 (2004)
15. Chen, X., Shen, S., Guo, L., Mao, S.S.: Semiconductor-based photocatalytic hydrogen generation. Chem. Rev. **110**, 6503–6570 (2010)
16. Wu, G., Chen, T., Zhou, G., Zong, X., Li, C.: H_2 production with low CO selectivity from photocatalytic reforming of glucose on metal/TiO_2 catalysts. Sci. China Ser. B Chem. **51**, 97–1000 (2008)
17. Primo, A., Corma, A., Garcia, H.: Titania supported gold nanoparticles as photocatalyst. Phys. Chem. Chem. Phys. **13**, 886–910 (2010)
18. Linic, S., Christopher, P., Ingram, D.: Plasmonic-metal nanostructures for efficient conversion of solar to chemical energy. Nat. Mater. **10**, 911–921 (2011)
19. Du, L., Furube, A., Yamamoto, K., Hara, K., Katoh, R., Tachiya, M.: Plasmon-induced charge separation and recombination dynamics in gold–TiO_2 nanoparticle systems: dependence on TiO_2 particle size. J. Phys. Chem. C **113**, 6454–6462 (2009)
20. Seh, Z.W., Liu, S., Low, M., Zhang, S.-Y., Liu, Z., Mlayah, A., Han, M.-Y.: Adv. Mater. **24**, 2310–2314 (2012)
21. Idriss, H., Wahab, A.K.: European Procedure (Patents) (12CHEM0012-EP-EPA) filed at the Patent Office on 03-09-2012 as Serial Number 12006217.9. (2012)
22. Bamwenda, G.R., Tsubota, S., Nakamura, T., Haruta, M.: Photoassisted hydrogen production from a water-ethanol solution: a comparison of activities of Au-TiO_2 and Pt-TiO_2. J. Photochem. Photobiol. A Chem. **89**, 177–189 (1995)
23. Sun, B., Vorontsov, V., Smirniotis, P.G.: Role of platinum deposited on TiO_2 in phenol photocatalytic oxidation. Langmuir **19**, 3151–3156 (2003)
24. Bamwenda, G.R., Tsubota, S., Kobayashi, T., Haruta, M.: Photoinduced hydrogen production from an aqueous solution of ethylene glycol over ultrafine gold supported on TiO_2. J. Photochem. Photobiol. A Chem. **77**, 59–67 (1994)
25. Sakata, T., Kawai, T.: Heterogeneous photocatalytic production of hydrogen and methane from ethanol and water. Chem. Phys. Lett. **80**, 341–344 (1981)
26. Yang, Y., Zhong, H., Tian, C.: Photocatalytic mechanisms of modified titania under visible light. Res. Chem. Intermed. **37**, 91–102 (2011)
27. Nair, R.G., Paul, S., Samdarshi, S.K.: High UV/visible light activity of mixed phase titania: a generic mechanism. Solar Energy Mater. Solar Cells **95**, 1901–1907 (2011)
28. Nadeem, M.A., Murdoch, M., Waterhouse, G.I.N., Metson, J.B., Keane, M.A., Llorca, J., Idriss, H.: Photoreaction of ethanol on Au/TiO_2 anatase: comparing the micro to nanoparticle size activities of the support for hydrogen production. J. Photochem. Photobiol. A Chem. **216**, 250–255 (2010)
29. Scott, M., Idriss, H.: Heterogeneous catalysis for hydrogen production. In: Anstis, P., Crabtree, R.H. (eds) Handbook of Green Chemistry—Green Catalysis, vol. 1, chap. 10, ISBN-10: 3-527-31577-2 (2009)
30. Idriss, H.: Ethanol reactions over the surfaces of transition metals/cerium oxide catalysts. Platin. Met. Rev. **48**, 105–115 (2004)
31. Murdoch, M., Waterhouse, G.I.N., Nadeem, M.A., Metson, J.B., Keane, M.A., Howe, R.F., Llorca, J., Idriss, H.: The effect of gold loading and particle size on photocatalytic hydrogen production from ethanol over Au/TiO_2 nanoparticles. Nat. Chem. **3**, 489–492 (2011)
32. Haruta, M.: Size- and support-dependency in the catalysis of gold. Catal. Today **36**, 153–166 (1997)
33. Valden, M., Lai, X., Goodman, D.W.: Onset of catalytic activity of gold clusters on titania with the appearance of non-metallic properties. Science **281**, 1647–1650 (1998)
34. Lai, X., Goodman, D.W.: Structure-reactivity correlations for oxide-supported metal catalysts: new perspectives from STM. J. Mol. Cat. A **162**, 33–50 (2000)
35. Cárdenas-Lizana, F., Gómez-Quero, S., Idriss, H., Keane, M.A.: Gold particle size effects in the gas phase hydrogenation of dinitrobenzene over Au/TiO_2. J. Catal. **268**, 223–234 (2009)
36. Li, G., Chen, L., Graham, M.E., Gray, K.A.: A comparison of mixed phase titania photocatalysts prepared by physical and chemical methods: the importance of the solid–solid interface. J. Mol. Cat. A. **275**, 30–35 (2007)
37. Kudo, A., Miseki, Y.: Heterogeneous photocatalyst materials for water splitting. Chem. Soc. Rev. **38**, 25–278 (2009)
38. Deak, P., Aradi, B., Frauenheim, T.: Band lineup and charge carrier separation in mixed rutile-anatase systems. J. Phys. Chem. C **115**, 3443–3446 (2011)
39. Kho, Y.K., Iwase, A., Teoh, W.Y., Madler, L., Kudo, A., Amal, R.: Photocatalytic H_2 evolution over TiO_2 nanoparticles. The synergistic effect of anatase and rutile. J. Phys. Chem. C. **114**, 2821–2829 (2010)
40. Long, R., Dai, Y., Huang, B.: Structural and electronic properties of iodine-doped anatase and rutile TiO_2. Comp. Mat. Sci. **45**, 223–228 (2009)
41. Lee, H.S., Woo, C.S., Youn, B.K., Kim, S.Y., Oh, S.T., Sung, Y.E., Lee, H.I.: Bandgap modulation of TiO_2 and its effects on

the activity in photocatalytic oxidation of 2-isopropyl-6-methyl-4-pyrimidinol. Top. Catal. **35**, 255–260 (2005)
42. Colbeau-Justin, C., Kunst, M.: Structural influence on charge-carrier lifetimes in TiO_2 powders studied by microwave absorption. J. Mater. Sci. **38**, 2429–2437 (2003)
43. Xu, M., Gao, Y., Moreno, E.M., Kunst, M., Muhler, M., Wang, Y., Idriss, H., Wöll, C.: Photocatalytic activity of bulk TiO_2 anatase and rutile single crystals using infrared absorption spectroscopy. Phys. Rev. Lett. **106**, 138302 (2011)
44. Shen, Q., Katayama, K., Sawada, T., Yamaguchi, M., Kumagai, Y., Toyoda, T.: Photoexcited hole dynamics in TiO_2 nanocrystalline films characterised using a lens-free heterodyne detection transient grating technique. Chem. Phys. Lett. **419**, 464–468 (2006)
45. Wilson, J.N., Idriss, H.: Structure sensitivity and photocatalytic reactions of semiconductors. Effect of the last layer atomic arrangement. J. Am Chem. Soc. **124**, 11284–11285 (2002)
46. Wilson, J.N., Idriss, H.: Effect of surface reconstruction of TiO_2(001) single crystal on the photoreaction of acetic acid. J. Catal. **214**, 46–52 (2003)
47. Komaguchi, K., Nakano, H., Araki, A., Harima, Y.: Photoinduced electron transfer from anatase to rutile in partially reduced TiO_2 (P-25) nanoparticles: an ESR study. Chem. Phys. Lett. **428**, 338–342 (2006)
48. Zhang, J., Xu, Q., Feng, M.L., Li, C.: Importance of the relationship between surface phases and photocatalytic activity of TiO_2. Agnew. Chem. Int. Ed. **47**, 1766–1769 (2008)
49. Bickley, R.I., Gonzalez-Carreno, T., Lees, J.S., Palmisano, L., Tilley, R.J.D.: A structural investigation of titanium dioxide photocatalysts. J. Sol. State Chem. **92**, 178–190 (1991)
50. Hurum, D.C., Agrios, A.G., Gray, K.A., Rajh, T., Thurnauer, M.C.: Explaining the enhanced photocatalytic activity of Degussa P25 mixed-phase TiO_2 using EPR. J. Phys. Chem. B **107**, 4545–4549 (2003)
51. Carneiro, J.T., Savenije, T.J., Moulijn, J.A., Mul, G.: How phase composition influences optoelectronic and photocatalytic properties of TiO_2. J. Phys. Chem. C **115**, 2211–2217 (2011)
52. Scott, M., Nadeem, A.M., Waterhouse, G.I.W., Idriss, H.: Hydrogen production from ethanol. Comparing thermal catalytic reactions to photo-catalytic reactions. MRS Proceed. **1326**, 1764–1769 (2011)
53. Hurum, D.C., Gray, K.A., Rajh, T., Thurnauer, M.C.: Recombination pathways in the Degussa P25 formulation of TiO_2: surface versus lattice mechanisms. J. Phys. Chem. B **109**, 977–980 (2005)
54. Scotti, R., D'Arienzo, M., Testino, A., Morazzoni, F.: Photocatalytic mineralization of phenol catalyzed by pure and mixed phase hydrothermal titanium dioxide. Appl. Catal. B **88**, 497–504 (2009)
55. Wahab, A.K., Waterhouse G.I.N., Hedhili, M., Anjum, D., Al-Hazza, A., Llorca, J., Idriss, H.: Hydrogen production from water over semiconductor materials: the role of synergism between different phases. American Chemical Society 244th meeting, August 2012 (USA) and Topics in Catalysis (in press)
56. Kandiel, T.A., Feldhoff, A., Robben, L., Dillert, R., Bahnemann, D.W.: Tailored titanium dioxide nanomaterials: anatase nanoparticles and brookite nanorods as highly active photocatalysts. Chem. Mater. **22**, 2050–2060 (2009)
57. Ismail, A.A., Kandiel, T.A., Bahnemann, D.W.: Novel (and better?) titania-based photocatalysts: brookite nanorods and mesoporous structures. J. Photochem. Photobiol. A Chem. **216**, 183–193 (2010)
58. Štengl, V., Králová, D.: Photoactivity of brookite–rutile TiO_2 nanocrystalline mixtures obtained by heat treatment of hydrothermally prepared brookite. Mater. Chem. Phys. **129**, 794–801 (2011)
59. Wang, C., Zhang, X., Shao, C., Zhang, Y., Yang, J., Sun, P., Liu, X., Liu, H., Liu, Y., Xie, T., Wang, D.: Rutile TiO_2 nanowires on anatase TiO_2 nanofibers: a branched heterostructured photocatalysts via interface-assisted fabrication approach. J. Coll. Interf. Sci. **363**, 157–164 (2011)
60. Xu, Q., Ma, Y., Zhang, J., Wang, X., Feng, Z., Li, C.: Enhancing hydrogen production activity and suppressing CO formation from photocatalytic biomass reforming on Pt/TiO_2 by optimizing anatase–rutile phase structure. J. Catal. **278**, 329–335 (2011)
61. Kim, S., Ehrman, S.H.: Photocatalytic activity of a surface-modified anatase and rutile titania nanoparticle mixture. J. Coll. Interf. Sci. **338**, 304–307 (2009)
62. Zhang, P., Yin, S., Sato, T.: A low-temperature process to synthesize rutile phase TiO_2 and mixed phase TiO_2 composites. Mater. Res. Bull. **45**, 275–278 (2010)